AGU PUBLICATIONS

Paleoceanography

RESEARCH ARTICLE
10.1002/2016PA003081

Key Points:
- Mid-depth Atlantic sequesters carbon during stadial events of the last deglaciation
- Carbon storage varies coherently with proxies of AMOC variability
- Storage and release of carbon from mid-depths may modulate atmospheric CO_2

Correspondence to:
D. Lund,
david.lund@uconn.edu

Citation:
Lacerra, M., D. Lund, J. Yu, and A. Schmittner (2017), Carbon storage in the mid-depth Atlantic during millennial-scale climate events, *Paleoceanography*, *32*, 780–795, doi:10.1002/2016PA003081.

Received 26 DEC 2016
Accepted 12 JUL 2017
Accepted article online 19 JUL 2017
Published online 3 AUG 2017

Carbon storage in the mid-depth Atlantic during millennial-scale climate events

Matthew Lacerra[1], David Lund[1], Jimin Yu[2], and Andreas Schmittner[3]

[1]Department of Marine Sciences, University of Connecticut, Storrs, Connecticut, USA, [2]Research School of Earth Sciences, Australian National University, Canberra, Australian Capital Territory, Australia, [3]College of Earth, Ocean, and Atmospheric Sciences, Oregon State University, Corvallis, Oregon, USA

Abstract Carbon isotope minima were a ubiquitous feature of the mid-depth Atlantic during Heinrich Stadial 1 (HS1, 14.5–17.5 kyr BP) and the Younger Dryas (YD, 11.5–12.9 kyr BP), yet their cause remains unclear. Recent evidence indicates that North Atlantic processes triggered the $\delta^{13}C$ anomalies, with weakening of the Atlantic Meridional Overturning Circulation (AMOC) being the most likely driver. Model simulations suggest that slowing of the AMOC increases the residence time of mid-depth waters in the Atlantic, resulting in the accumulation of respired carbon. Here we assess ΣCO_2 variability in the South Atlantic using benthic foraminiferal B/Ca, a proxy for $[CO_3^{2-}]$. Using replicated high-resolution B/Ca records from ~2 km water depth on the Brazil Margin, we show that $[CO_3^{2-}]$ decreased during HS1 and the YD, synchronous with apparent weakening of the AMOC. The $[CO_3^{2-}]$ response is smaller than in the tropical North Atlantic during HS1, indicating there was a north–south gradient in the $[CO_3^{2-}]$ signal similar to that for $\delta^{13}C$. The implied variability in ΣCO_2 is consistent with model results, suggesting that carbon is temporarily sequestered in the mid-depth Atlantic during millennial-scale stadial events. Using a carbon isotope mass balance, we estimate that approximately 75% of the HS1 $\delta^{13}C$ signal at the Brazil Margin was driven by accumulation of remineralized carbon, highlighting the nonconservative behavior of $\delta^{13}C$ during the last deglaciation.

Plain Language Summary The rise in atmospheric CO_2 between the last ice age and the current interglacial period is the most recent example of natural CO_2 variability driving changes in Earth's climate. It is generally believed that atmospheric CO_2 increased due to the release of carbon from the deep ocean. Here we show that the mid-depth (1.5–2.5 km) Atlantic temporarily stored carbon during the deglaciation while atmospheric CO_2 was rising. Our results suggest that the mid-depth Atlantic was not a persistent source of carbon during the last deglaciation and that other factors must have accounted for rising atmospheric CO_2 levels.

1. Introduction

The last deglaciation (10–18 kyr BP) was characterized by major changes in the Earth's climate system, including a 120 m rise in global sea level [*Clark et al.*, 2009], a ~4°C increase in average surface temperature [*Shakun et al.*, 2012; *Annan and Hargreaves*, 2013], and an 80 ppmv increase in atmospheric CO_2 [*Marcott et al.*, 2014]. Given that global temperature tracked CO_2 levels [*Shakun et al.*, 2012] and that greenhouse gases are necessary to simulate the full deglacial temperature rise [*Weaver et al.*, 1998; *Schneider et al.*, 2010], isolating the mechanisms that regulate atmospheric CO_2 is essential to understanding Earth's transition from a glacial to interglacial state.

The initial changes in deglacial climate occurred during Heinrich Stadial 1 (HS1, 14.5–17.5 kyr BP), including a 30 ppmv rise in pCO_2 and a decrease in the $\delta^{13}C$ of CO_2 of 0.3–0.4‰ [*Lourantou et al.*, 2010; *Schmitt et al.*, 2012; *Bauska et al.*, 2016]. Foraminiferal records also show that decreases in $\delta^{13}C$ were widespread in the surface and mid-depth (1.5–2.5 km) Atlantic Ocean [*Curry et al.*, 1988; *Schneider et al.*, 1992; *Oppo et al.*, 2015]. The largest anomalies occurred in the subpolar North Atlantic [*McManus et al.*, 1999; *Rickaby and Elderfield*, 2005; *Praetorius et al.*, 2008], with progressively smaller $\delta^{13}C$ excursions in the tropical [*Zahn and Stüber*, 2002; *Oppo and Fairbanks*, 1987] and South Atlantic [*Tessin and Lund*, 2013; *Lund et al.*, 2015]. The timing of the mid-depth $\delta^{13}C$ signals is similar to the atmospheric $\delta^{13}C$ anomaly, suggesting that circulation changes in the Atlantic played a key role in spurring the initial rise of atmospheric CO_2 during the last deglaciation [*Oppo et al.*, 2015; *Schmittner and Lund*, 2015].

Several mechanisms have been proposed to explain HS1 $\delta^{13}C$ anomalies in the Atlantic, including regional brine formation [*Dokken and Jansen*, 1999; *Thornalley et al.*, 2010; *Waelbroeck et al.*, 2011], greater incursion of Antarctic Intermediate Water (AAIW) [*Rickaby and Elderfield*, 2005], and weakening of the Atlantic Meridional Overturning Circulation (AMOC) [*Zahn et al.*, 1997]. Although the abyssal South Atlantic was depleted in ^{13}C during the Last Glacial Maximum (LGM) [*Duplessy et al.*, 1988; *Curry and Oppo*, 2005; *Hoffman and Lund*, 2012], it is an unlikely source of mid-depth anomalies because the $\delta^{13}C$ signal in the abyssal and mid-depth records is offset by several thousand years [*Lund et al.*, 2015]. Moreover, the idea that greater incursion of AAIW caused the HS1 minima is now considered unlikely, as new records suggest a reduced presence of AAIW in the North Atlantic during this time [*Xie et al.*, 2012; *Huang et al.*, 2014]. Greater incursion of AAIW should also lead to lower $\delta^{13}C$ at intermediate depths, which is opposite the pattern observed at multiple sites in the Southern Hemisphere, including the Brazil Margin [*Hertzberg et al.*, 2016]. Instead, the mid-depth anomalies are most likely due to a change in the isotopic composition of Northern Component Water (NCW) [*Oppo et al.*, 2015]. The end-member $\delta^{18}O$ and $\delta^{13}C$ values for NCW exhibited a significant change during the LGM-HS1 transition (-1.2‰ and -1.0‰, respectively), while end-member values for deep southern sourced water remained relatively stable [*Lund et al.*, 2015]. Cross plots of benthic $\delta^{13}C$ versus $\delta^{18}O$ suggest that mid-depth Brazil Margin sites fall on a mixing line between NCW and deep (2500–3000 m) southern component water during HS1, implying that variable NCW composition caused the mid-depth anomalies [*Lund et al.*, 2015]. Similarly, a compilation of Atlantic LGM $\delta^{13}C$ versus LGM-HS1 $\delta^{13}C$ indicates that NCW was the primary driver of the HS1 signal (see Figure 5 in *Oppo et al.* [2015]).

Model simulations suggest that the shift in NCW during HS1 was due to a severe reduction in the AMOC. Shutdown of the AMOC by freshwater forcing in the North Atlantic yields negative $\delta^{13}C$ anomalies at mid-depth, with the largest signal occurring in the high latitude North Atlantic and progressively smaller anomalies in the tropical and South Atlantic, similar to the observed spatial trend during HS1 [*Schmittner and Lund*, 2015]. The $\delta^{13}C$ response is due to reduced sinking of high $\delta^{13}C$ surface water in the North Atlantic and increased residence time of deep water, which allows for the accumulation of isotopically light respired carbon. Under modern conditions, the North Atlantic has high $\delta^{13}C$ values due to sinking of ^{13}C-enriched surface waters and rapid transport of deep water by the AMOC, while the South Atlantic has lower $\delta^{13}C$ due to mixing with ^{13}C-depleted Upper Circumpolar Deep Water and Antarctic Bottom Water [*Kroopnick*, 1985; *Schmittner et al.*, 2013]. The simulated shutdown of the AMOC nearly eliminates this gradient, making the Atlantic $\delta^{13}C$ tracer field similar to the modern deep Pacific where remineralization is the primary driver of $\delta^{13}C$ variability [*Schmittner and Lund*, 2015].

Although the modeled Atlantic response generally agrees with the observed spatial pattern in $\delta^{13}C$ anomalies, the simulated signal in the North Atlantic is approximately 50% larger than in the benthic $\delta^{13}C$ records. Bioturbation may mute the reconstructed signal in low sedimentation rate locations, but both high and low resolution records yield smaller than predicted anomalies in the North Atlantic [*Schmittner and Lund*, 2015]. The discrepancy may instead be related to the initial conditions used in the AMOC simulations, which were based on a preindustrial rather than LGM climate state. Another possibility is that the Atlantic overturning did not fully collapse during HS1. While initial $^{231}Pa/^{230}Th$ records from the North Atlantic pointed toward a complete AMOC shutdown [*McManus et al.*, 2004], newer results are consistent with the continued export of ^{231}Pa out of the North Atlantic [*Gherardi et al.*, 2009]. Furthermore, the Pa/Th proxy is influenced by spatially variable particle scavenging, indicating that it may not be a direct quantitative indicator of AMOC flux [*Hayes et al.*, 2015].

A key unknown is whether the mid-depth carbon isotope anomalies were driven by changes in preformed or remineralized carbon. If temperature dependent air-sea equilibration [e.g., *Lynch-Stieglitz et al.*, 1995] was the primary driver of the $\delta^{13}C$ signal, we would expect little change in ΣCO_2 at mid-depths. On the other hand, a substantial increase in ΣCO_2 would point to either (1) accumulation of respired carbon, due to weakening of the AMOC, or (2) higher preformed DIC, due to rising atmospheric CO_2. If it was the former, we would expect higher ΣCO_2 during HS1 and lower ΣCO_2 during the Bølling-Allerød (B-A, 12.9–14.5 kyr BP), whereas the latter should yield a monotonic increase in ΣCO_2 during the deglaciation. One existing record from the tropical North Atlantic (~12°N; 1800 m) shows that $[CO_3^{2-}]$ decreased by ~30 μmol/kg during the LGM-HS1 transition and remained low into the Holocene [*Yu et al.*, 2010]. Assuming alkalinity (ALK) remained constant and $[CO_3^{2-}] \approx 0.6 * (ALK - \Sigma CO_2)$ [*Yu et al.*, 2016], these results suggest that ΣCO_2 increased by ~50 μmol/kg,

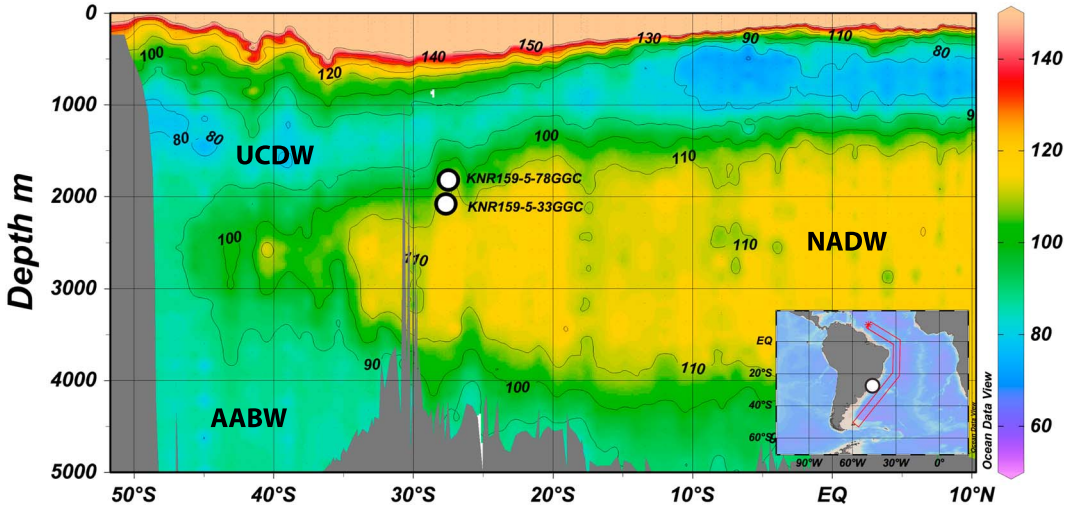

Figure 1. Locations of cores used in this study (white circles) overlain on a cross section of carbonate ion concentration (in μmol/kg) from World Ocean Circulation Experiment (WOCE) A17 [*Schlitzer*, 2015]. Contour intervals are 10 μmol/kg. The sites are influenced primarily by high [CO_3^{2-}] North Atlantic Deep Water (NADW) and to a lesser extent low [CO_3^{2-}] Upper Circumpolar Deep Water (UCDW). The inset map shows the location of the A17 section relative to the core sites (white circles). Note that hydrographic data closer to the core sites were used to estimate the modern carbonate ion values depicted in Figure 2 (see section 2.3).

which is inconsistent with temperature-dependent fractionation causing the mid-depth $\delta^{13}C$ anomalies. However, it leaves open the possibility that the [CO_3^{2-}] signal was driven by preformed DIC. One of the goals of this work is to verify the North Atlantic results using new records from locations influenced by the AMOC that are capable of resolving millennial-scale [CO_3^{2-}] variability.

Here we reconstruct [CO_3^{2-}] in the Southwest Atlantic using B/Ca analyses of benthic foraminifera from two mid-depth cores on the Brazil Margin (at 1.8 and 2.1 km water depth; Figure 1). During the LGM, water at these depths was approximately 70% NCW and 30% Antarctic Bottom Water [*Tessin and Lund*, 2013; *Curry and Oppo*, 2005], while during the Holocene the primary end-member influences were NADW and UCDW [*Hoffman and Lund*, 2012]. The cores have accumulation rates of ~30 cm/kyr, which allows for high-resolution (200–300 years) reconstruction of [CO_3^{2-}], which we use to infer changes in ΣCO_2. We use [CO_3^{2-}] estimates and $\delta^{13}C$ records from the same cores to infer the preformed and remineralized components of the HS1 $\delta^{13}C$ anomalies. We also evaluate the Brazil Margin records in the context of [CO_3^{2-}] and circulation proxies from the North Atlantic to assess the relative timing of events and whether variable AMOC strength drove changes in carbon storage at mid-depth. Finally, we discuss the implications of our findings as they relate to the HS1 carbon isotope minima and centennial to millennial-scale changes in atmospheric CO_2. It has been hypothesized that release of stored carbon due to reinvigoration of the AMOC may explain the abrupt 10–15 ppm increases in atmospheric CO_2 at the end of HS1 and the Younger Dryas (YD) [*Chen et al.*, 2015]. One objective of this study is to assess whether carbon was temporarily sequestered in the mid-depth Atlantic using the Brazil Margin records.

2. Methods

2.1. Core Sampling

Sediment samples were taken from two cores on the Brazil Margin, KNR159-5-78GGC (1820 m; 27.5°S, 46.3°W) and KNR159-5-33GGC (2082 m; 27.6°S, 46.2°W). In core 78GGC, samples were collected at 2 cm intervals from the core top to 61 cm, and then 4 cm intervals from 61 to 201 cm (for a total of 68 samples). Two of the samples (at 73 and 77 cm) were collected within the bioturbated interval from 70 to 80 cm [*Tessin and Lund*, 2013]. Note that this interval occurs after the decline in $\delta^{13}C$ and [CO_3^{2-}] at the beginning of HS1. We collected a total of 42 samples from 33GGC, ranging from 2 cm intervals from the core top to 59 cm and then 4 cm intervals from 59 to 199 cm, with the exception of 118 to 143 cm, where the average sampling interval was 12 cm.

Table 1. Parameters for Estimating Modern Brazil Margin [CO_3^{2-}]

Core	Water Depth (m)	Potential Temp (°C)	S	PO_4^{3-} (μmol/kg)	SiO_3^{2-} (μmol/kg)	ALK (μmol/kg)	Avg. ΣCO_2 (μmol/kg)	[CO_3^{2-}] (μmol/kg)
78GGC	1820	3.81	34.90	1.7	30	2310 ± 5	2185 ± 7	94 ± 7
33GGC	2082	3.50	34.95	1.5	25	2312 ± 9	2171 ± 2	102 ± 7

The varied sample spacing in each core was necessary to compensate for generally lower sedimentation rates in the Holocene and late deglacial sections of each core. The upper 50 cm of 78GGC has sedimentation rates of 3 cm/kyr, while below 50 cm the rate is approximately 35 cm/kyr [*Tessin and Lund*, 2013]. Similarly, sedimentation rates in the upper 75 cm of core 33GGC are 2 cm/kyr, while deeper in the core the rate is ~27 cm/kyr. In total, we collected 86 samples from 78GGC and 51 samples from core 33GGC for B/Ca analyses. Samples were freeze-dried, washed through a 150 μm sieve, and dried at 40°C overnight.

2.2. B/Ca

B/Ca analyses were performed on the benthic foraminifer *Cibicidoides wuellerstorfi* in the laboratory of Dr. Jimin Yu at Australian National University. *C. wuellerstorfi* were taken from the >250 μm size fraction with five to eight tests used for each B/Ca analysis. Samples were crushed using glass microscope slides with just enough force to rupture individual chambers. A compound light microscope was used to facilitate the crushing procedure and the removal of exceptionally dirty chambers. The crushed samples were rinsed into sample vials using Milli-Q water and ultrasonicated for 30 s to bring any clay material into suspension. The mixture was then stirred by squirting Milli-Q into each vial. After test fragments had resettled, the overlying fluid was pipetted out. This procedure was repeated with Milli-Q and then methanol rinses until sonication yielded a clear, particle-free supernatant. Using a high powered reflected-light microscope, we used a single haired picking brush to remove pyrite and other foreign materials from test fragments that remained after the rinsing procedure. The samples then underwent oxidative cleaning to remove organic matter using a buffered H_2O_2 solution (100 μL 30%*v/v* H_2O_2 + 10 mL 0.1 M NaOH). The final step of the cleaning protocol involved leaching using a weak acid solution (0.001 M HNO_3). Cleaned samples were analyzed for B/Ca using a Varian ICP 820MS. The analytical precision for the 150 μmol/mol B/Ca consistency standard analyzed with the unknowns was 1.6% (n = 16). Full details of the analytical procedure can be found in *Yu and Elderfield* [2005].

2.3. [CO_3^{2-}] and ΣCO_2

Modern carbonate ion concentrations for the Brazil Margin were estimated using the local and regional hydrographic parameters listed in Table 1. Potential temperature and salinity values were taken directly from cruise KNR159-5 CTD data. PO_4^{3-} and SiO_3^{2-} values were estimated using WOCE Atlas Volume 3, section A10, which intersects the Brazil Margin at 28°S (http://whpatlas.ucsd.edu/whp_atlas/atlantic/a10/sections/sct_menu.htm). ALK and ΣCO_2 values were estimated using WOCE data from stations 13003 (43.58°W, 28.83°S) and 13627 (46.48°W, 27.95°S), located approximately 300 and 60 km from the core sites, respectively (http://www.ewoce.org/data/index.html#WHP_Bottle_Data). Given sloping isopycnals between the WOCE stations and the core locations, ALK and ΣCO_2 values were estimated using station data within ±0.05 kg/m^3 of the potential density at each core site. Using the data in Table 1, we then estimated [CO_3^{2-}] using CO2SYS_v1.1 [*Lewis et al.*, 2014]. Carbonate ion saturation values were determined using the equation $[CO_3^{2-}]_{sat} = [CO_3^{2-}]/\Omega_{calcite}$, where $\Omega_{calcite}$ is the saturation state for calcite at the depth of each core.

Down core estimates of [CO_3^{2-}] were determined using a B/Ca to $\Delta[CO_3^{2-}]$ conversion of 1.14 (μmol/mol) B/Ca per (μmol/kg) $\Delta[CO_3^{2-}]$ [*Yu and Elderfield*, 2007]. This relationship is based on a global core-top calibration for *C. wuellerstorfi*. We then estimated [CO_3^{2-}] using the relationship $[CO_3^{2-}] = \Delta[CO_3^{2-}] + [CO_3^{2-}]_{sat}$, where $[CO_3^{2-}]_{sat}$ is based on modern hydrographic conditions and water depths (Table 1). Our estimates of ΣCO_2 are based on the carbonate alkalinity relationship $\Sigma CO_2 \approx ALK - [CO_3^{2-}]/0.6$ [*Yu et al.*, 2016]. We assume that [CO_3^{2-}] primarily responds to changing ΣCO_2 but also discuss the moderating influence that alkalinity may play on millennial and longer time scales. To create a representative time series for the Brazil Margin sites for comparison to other paleoclimate proxies, we combined the [CO_3^{2-}] results from each core into a single time series and then plotted the results using a simple 3-point running mean.

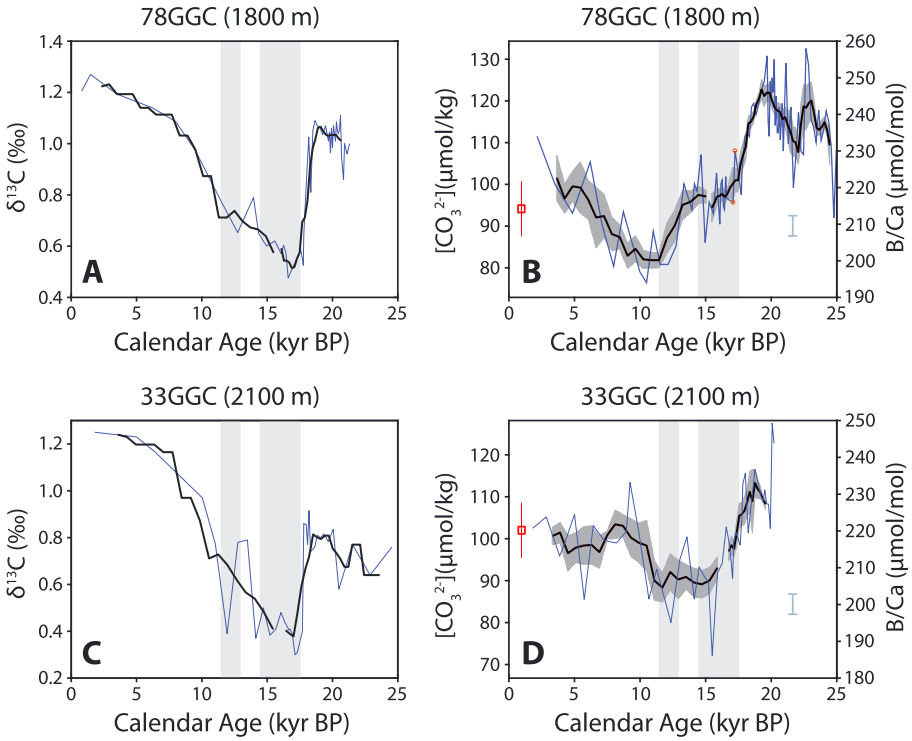

Figure 2. Brazil Margin $\delta^{13}C$ and B/Ca records spanning the LGM through late Holocene. (a) *C. wuellerstorfi* $\delta^{13}C$ data for KNR159-5-78GGC, including the average value at each stratigraphic level (thin blue line), a 3000 year running mean from 2 to 16 kyr BP, and a 1000 year running mean from 16 to 25 kyr BP (thick black lines). A wider averaging window was necessary from 2 to 16 kyr BP due to the lower sedimentation rates in the late deglaciation and Holocene. Stable isotope and radiocarbon data are from *Tessin and Lund* [2013] with calibrated dates as in *Lund et al.* [2015]. (b) Benthic B/Ca data for KNR159-5-78GGC (right *y* axis), including the average value at each stratigraphic level (thin blue line), running mean values as in Figure 2a, and ±1 SE uncertainties (shaded area). Carbonate ion concentrations (left *y* axis) were estimated using a core top calibration of 1.14 μmol/mol B/Ca per μmol/kg $[CO_3^{2-}]$, with a calibration uncertainty of 5 μmol/kg = 1σ [*Yu et al.*, 2016], shown as the blue-gray error bar. Note that data points at 73 and 77 cm (red circles) are from a bioturbated section of the core (see text for details). (c and d) Benthic $\delta^{13}C$ and B/Ca data for KNR159-5-33GGC. The averaging window in Figure 2c is a 4000 year running mean from 2 to 16 kyr BP and a 2000 year running mean from 16 to 25 kyr BP. The red squares in Figures 2b and 2d are estimates of modern $[CO_3^{2-}]$ for the Brazil Margin sites (Table 1). The vertical red bars are ±1σ uncertainties. The vertical gray bars in each panel mark the HS1 (14.5–17.5 kyr BP) and YD (11.6–12.9 kyr BP) intervals.

3. Results

3.1. $[CO_3^{2-}]$ Data

Benthic foraminiferal $[CO_3^{2-}]$ time series for the Brazil Margin show similar overall patterns on glacial-interglacial time scales (Figure 2). At 1800 and 2100 m, $[CO_3^{2-}]$ is highest during the late LGM (19–21 kyr BP), with values of 122 ± 2 and 108 ± 1 μmol/kg, respectively. (Unless otherwise noted, the uncertainties stated here are standard errors.) Higher implied $[CO_3^{2-}]$ values at 1800 m during the LGM are consistent with the presence of well ventilated Glacial North Atlantic Intermediate Water above ~2 km water depth [*Curry and Oppo*, 2005; *Yu et al.*, 2008; *Hoffman and Lund*, 2012]. At 18 kyr BP, $[CO_3^{2-}]$ began to decrease at both sites, reaching a minimum of ~85 μmol/kg by 12 kyr BP, and then rebounding at ~10 kyr BP. At 2100 m, the increase is abrupt and then levels off by 8 kyr BP, whereas at 1800 m, $[CO_3^{2-}]$ continues to increase gradually throughout the Holocene. Given the more variable $[CO_3^{2-}]$ results at 2100 m after 10 kyr BP, additional data are necessary to better constrain the time series during this interval. Nonetheless, the results from both cores converge to a similar $[CO_3^{2-}]$ value (~100 μmol/kg) in the late Holocene. The core top results are similar to modern Brazil Margin $[CO_3^{2-}]$ values at 1800 and 2100 m (Figures 2b and 2d), even though the ALK and ΣCO_2 station data used to calculate modern $[CO_3^{2-}]$ are well offshore of the Brazil Margin core sites and the late Holocene data are relatively sparse in each core.

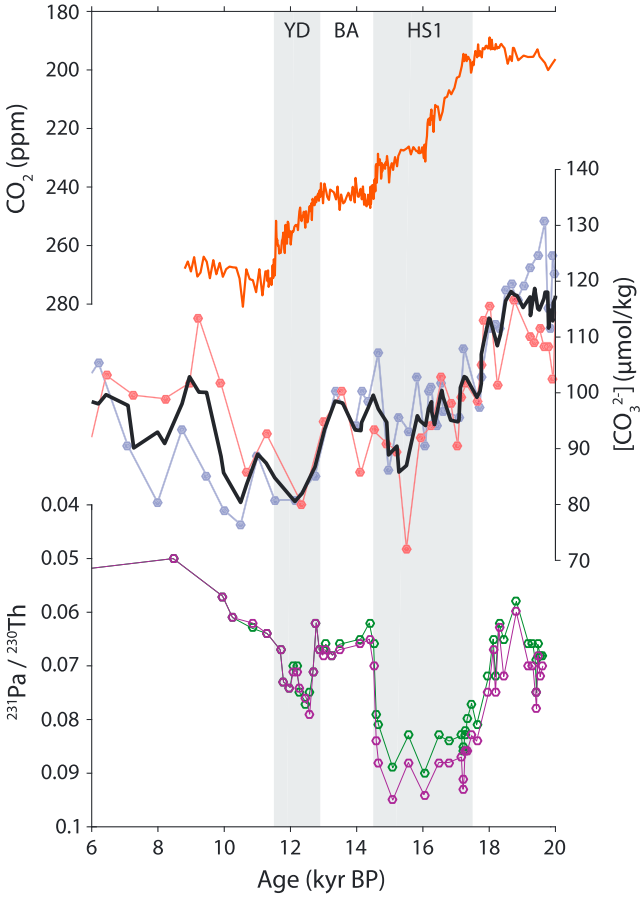

Figure 3. Atmospheric CO_2, Brazil Margin carbonate ion, deep North Atlantic $^{231}Pa/^{230}Th$ results. (a) Atmospheric CO_2 record [*Marcott et al.*, 2014] with updated WD2014 age scale [*Sigl et al.*, 2016]. Note that *y* axis is reversed. (b) Brazil Margin $[CO_3^{2-}]$ records for cores 78GGC (blue circles) and 33GGC (red circles) and a 3-point running mean of the combined 78GGC and 33GGC records (black line). (c) Sedimentary $^{231}Pa/^{230}Th$ data for OCE326-GGC5 (33°N, 4.5 km) including ^{238}U-based values (purple circles) and ^{232}Th-based values (green circles). The solid green bar and blue bar delineate the HS1 (14.5–17.5 kyr BP) and YD intervals (11.6–12.9 kyr BP), respectively. The Pa/Th and $[CO_3^{2-}]$ results are consistent with a weakened AMOC during HS1, strengthening during the B-A, and then weakening during the YD.

Millennial-scale changes in $[CO_3^{2-}]$ are apparent throughout the deglaciation. Between the late LGM (19–21 kyr BP) and early HS1 (16–17 kyr BP), $[CO_3^{2-}]$ decreased 22 ± 2 μmol/kg at 1800 m and 14 ± 4 μmol/kg at 2100 m (Figures 2 and 3). During the HS1 to B-A transition, $[CO_3^{2-}]$ at 1800 and 2100 m increased by ~15 μmol/kg and then decreased by a similar amount at the beginning of Younger Dryas (YD: 11.5–12.9 kyr BP). The average $[CO_3^{2-}]$ record ($[CO_3^{2-}]_{AVG}$) shows a pattern similar to individual time series (Figure 3). The main exception is the early Holocene, where deepening of NCW apparently caused the individual records to diverge (see section 4.7).

3.2. $[CO_3^{2-}]$ Versus $\%CaCO_3$

Calcium carbonate results from 78GGC and 33GGC provide additional perspective on changes in bottom water carbonate chemistry during the deglaciation (Figure 4). $\%CaCO_3$ values ranged from 10 to 15% in the 20 to 16 kyr BP interval, followed by an increase to 40% by 10 kyr BP, and then a slight decrease during the Holocene (Figures 4a and 4c). Thus, the long-term trend in $\%CaCO_3$ is generally opposite that for $[CO_3^{2-}]$ in each core. The difference is due to dilution of $CaCO_3$ by noncarbonate sedimentary components. $\%CaCO_3$ is suppressed during the LGM and early deglaciation due to input of hemipelagic clays that yield sedimentation rates an order of magnitude higher than during the Holocene [*Tessin and Lund*, 2013]. During the early deglaciation, however, sedimentation rates in 78GGC and 33GGC are nearly constant. The 1–3% decrease in $\%CaCO_3$ during HS1 may therefore reflect calcium carbonate dissolution (Figures 4b and 4d). The synchronous decrease in $\%CaCO_3$ and $[CO_3^{2-}]$ during HS1 suggests that higher ΣCO_2 at 1800–2100 m water depth resulted in modest calcite dissolution, which would tend to increase alkalinity locally.

4. Discussion

Our primary aim in reconstructing the carbonate ion history at the Brazil Margin is to elucidate changes in South Atlantic carbon cycling. In particular, our goal is to determine whether the mid-depth Atlantic acted as a temporary reservoir of carbon during millennial-scale stadial events of the last deglaciation, as predicted by modeling results [*Schmittner and Lund*, 2015]. Below we discuss changes in mid-depth South Atlantic

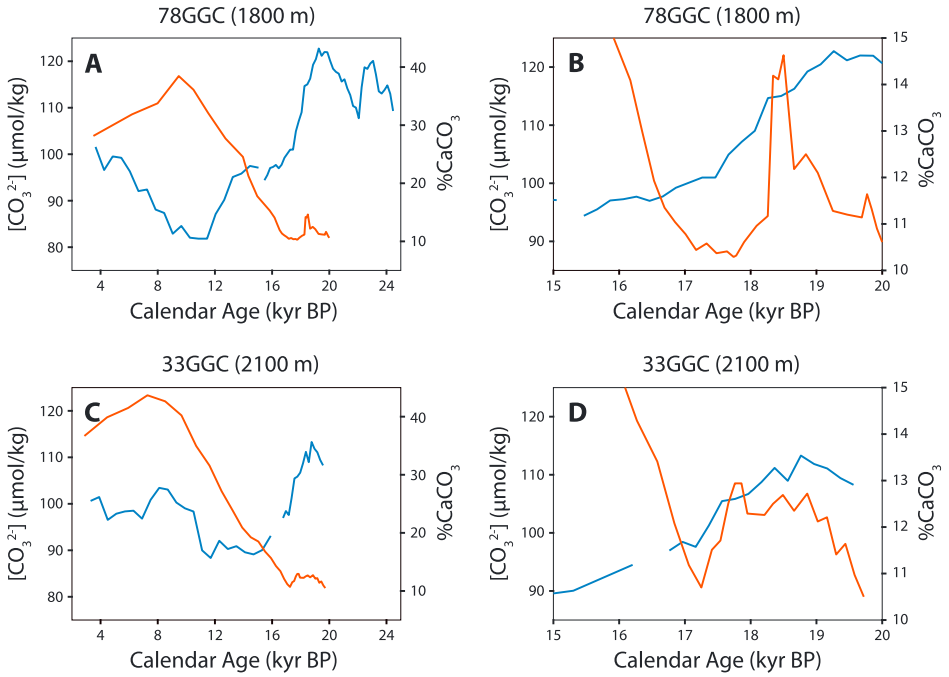

Figure 4. Brazil Margin [CO_3^{2-}] (blue lines) and %$CaCO_3$ records (orange lines). [CO_3^{2-}] is plotted as in Figure 2 and %$CaCO_3$ is plotted as a three-point running mean. (a) [CO_3^{2-}] and %$CaCO_3$ records for KNR159-5-78GGC spanning 2 to 25 kyr BP. (b) Zoomed in view of Figure 4a spanning 15 to 20 kyr BP. (c and d) Same as Figures 4a and 4b but for KNR159-5-33GGC. The long-term trends in %$CaCO_3$ reflect variable sedimentation rate at the Brazil Margin due to input of hemipelagic clay [*Tessin and Lund*, 2013], while the narrower windows highlight short-term changes that are more likely dependent on ΣCO_2.

[CO_3^{2-}] during HS1, the B-A, and YD, as well as broader, glacial-interglacial trends, with the purpose of highlighting variability across a range of time scales. We also discuss the most likely mechanisms behind the observed changes in [CO_3^{2-}], use mass balance constraints to assess the remineralized versus preformed components of the HS1 $\delta^{13}C$ signal, and make an initial estimate of carbon sequestration in the mid-depth Atlantic during HS1.

4.1. Millennial-Scale Signal Driven by Variable Carbon Storage

Both Brazil Margin time series suggest that [CO_3^{2-}] decreased by ~20 µmol/kg during HS1 (Figure 2). Given that [CO_3^{2-}] is a function of both alkalinity and total dissolved inorganic carbon, it is possible the [CO_3^{2-}] signal reflects decreasing ALK. We believe this is unlikely, however, given that average oceanic alkalinity would have a lagged response to any deglacial changes in carbonate preservation, particularly if they were related to sea level rise, the bulk of which occurred after HS1 [*Clark et al.*, 2009]. Additionally, %$CaCO_3$ at the Brazil Margin decreased slightly at 1800 and 2100 m water depth during HS1 (Figure 4), which would increase alkalinity locally, opposite the effect required to account for the [CO_3^{2-}] signal. Finally, modeling results indicate that weakening of the AMOC increases alkalinity at mid-depths (Figure 5). The continued export of $CaCO_3$ from the surface ocean and its dissolution in the deep ocean, combined with a more sluggish circulation, increases [Ca^{2+}] and therefore alkalinity. The modeled ALK increase at the Brazil Margin is approximately 20 µM, which yields an equivalent increase in [CO_3^{2-}]. Thus, the reconstructed [CO_3^{2-}] decline during HS1 may underestimate the ΣCO_2 signal.

The mid-depth $\delta^{13}C$ anomalies at the Brazil Margin were most likely driven by weakening of the AMOC [*Lund et al.*, 2015; *Oppo et al.*, 2015; *Schmittner and Lund*, 2015]. Therefore, the simplest explanation of the [CO_3^{2-}] signal also involves the AMOC, either through higher preformed DIC values in the source region or accumulation of respired carbon due to increased residence time of mid-depth waters. While

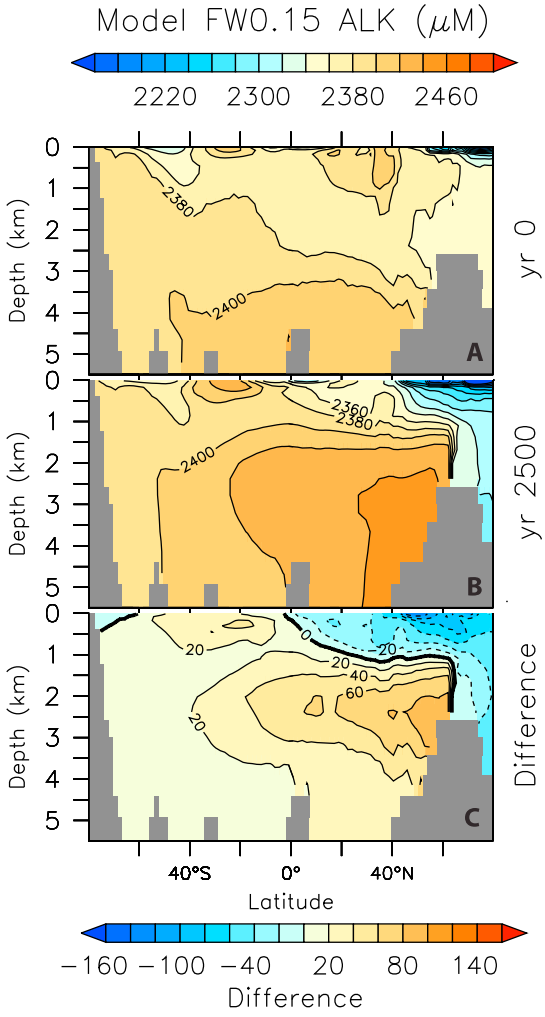

Figure 5. Simulated Atlantic Ocean alkalinity response due to a freshwater forcing induced AMOC shutdown [*Schmittner and Lund*, 2015]. (a) Alkalinity for the preindustrial control run. (b) Alkalinity 2500 years after AMOC shutdown. (c) The difference between the preindustrial control and the shutdown state.

the first option appears to be plausible, in part because the decrease in Brazil Margin $[CO_3^{2-}]$ and the initial increase in atmospheric CO_2 both occurred during HS1, closer examination of the records reveals that the $[CO_3^{2-}]$ signal leads atmospheric CO_2 by ~1 kyr (Figure 3). If air-sea gas exchange was responsible for increased ΣCO_2 in the mid-depth Atlantic, then $[CO_3^{2-}]$ at the Brazil Margin would lag or be contemporaneous with atmospheric CO_2. The age error for the ice core CO_2 record at ~17 kyr BP is ±80 years (1σ) [*Sigl et al.*, 2016]. The age error for the Brazil Margin data at 18 kyr BP is ±250 years (1σ) [*Tessin and Lund*, 2013], which is primarily due to an assumed ±200 year uncertainty in surface water reservoir age. Reconciling the Brazil Margin and atmospheric CO_2 time series would require a 1000 year increase in reservoir age, an unrealistically large change given the subtropical gyre location of the Brazil Margin sites (modern $\Delta R = 7 \pm 59$ years (1σ)) [*Angulo et al.*, 2005]. Furthermore, the increase in $[CO_3^{2-}]$ at the end of HS1 is not matched by a decrease in atmospheric CO_2 (Figure 3), suggesting that preformed DIC levels were not a primary driver of millennial-scale $[CO_3^{2-}]$ variability at the Brazil Margin.

4.2. Temporary Carbon Storage Driven by AMOC Variability

If AMOC weakening and accumulation of respired carbon drove the $[CO_3^{2-}]$ signal, the B/Ca records should display variability similar to proxies of the AMOC. The $^{231}Pa/^{230}Th$ record of *McManus et al.* [2004] is commonly used as a reference time series for AMOC variability. Given the caveats associated with Pa/Th as a circulation proxy [e.g., *Gherardi et al.*, 2009; *Hayes et al.*, 2015], here we use it to assess the approximate timing of changes in the AMOC rather than a quantitative measure of AMOC strength. Given that the overall pattern in Pa/Th is consistent with other circulation proxies from the Atlantic [*Chen et al.*, 2015; *Tessin and Lund*, 2013; *Oppo et al.*, 2015], we believe such an approach is reasonable. At the beginning of HS1, $[CO_3^{2-}]$ at the Brazil Margin decreased concomitantly with the rise in Pa/Th, suggesting that a weaker AMOC not only reduced export of Pa from the North Atlantic but also led to increased carbon storage and lower $[CO_3^{2-}]$ at the Brazil Margin (Figure 3). While Pa/Th remained relatively stable from 17 to 15 kyr BP, $[CO_3^{2-}]$ in both Brazil Margin cores continued to decrease after 16 kyr BP, which may reflect continued accumulation of respired carbon in a weakened AMOC state or a delayed response to rising atmospheric CO_2. Results from the North Atlantic also show a decrease in $[CO_3^{2-}]$ at the onset of HS1, but the record lacks the necessary resolution to determine whether $[CO_3^{2-}]$ continued to decline from 17 to 15 kyr BP [*Yu et al.*, 2010].

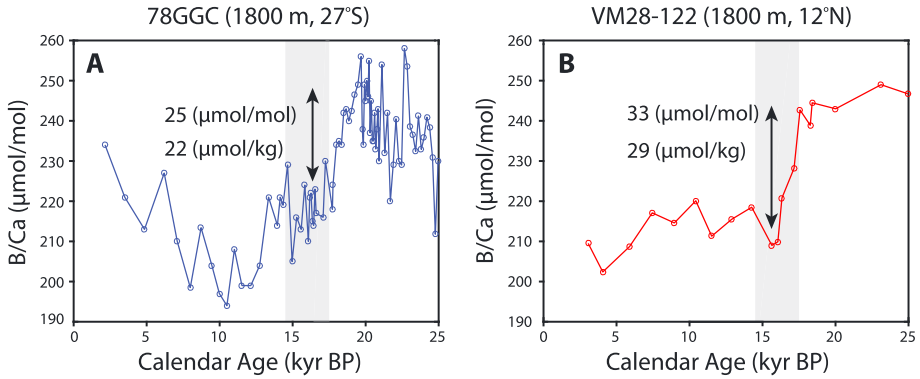

Figure 6. Brazil Margin and tropical North Atlantic B/Ca records spanning the LGM to late Holocene. (a) Benthic B/Ca data for KNR159-5-78GGC (blue circles). (b) Benthic B/Ca data for VM28-122 (red circles). [CO_3^{2-}] decreased ~20 μmol/kg at 27°S compared to ~30 μmol/kg at 12°N. The lower sedimentation rate for VM28-122 (7 cm/kyr during the deglaciation compared to 35 cm/kyr for 78GGC) likely yields a relatively muted B/Ca signal in the North Atlantic.

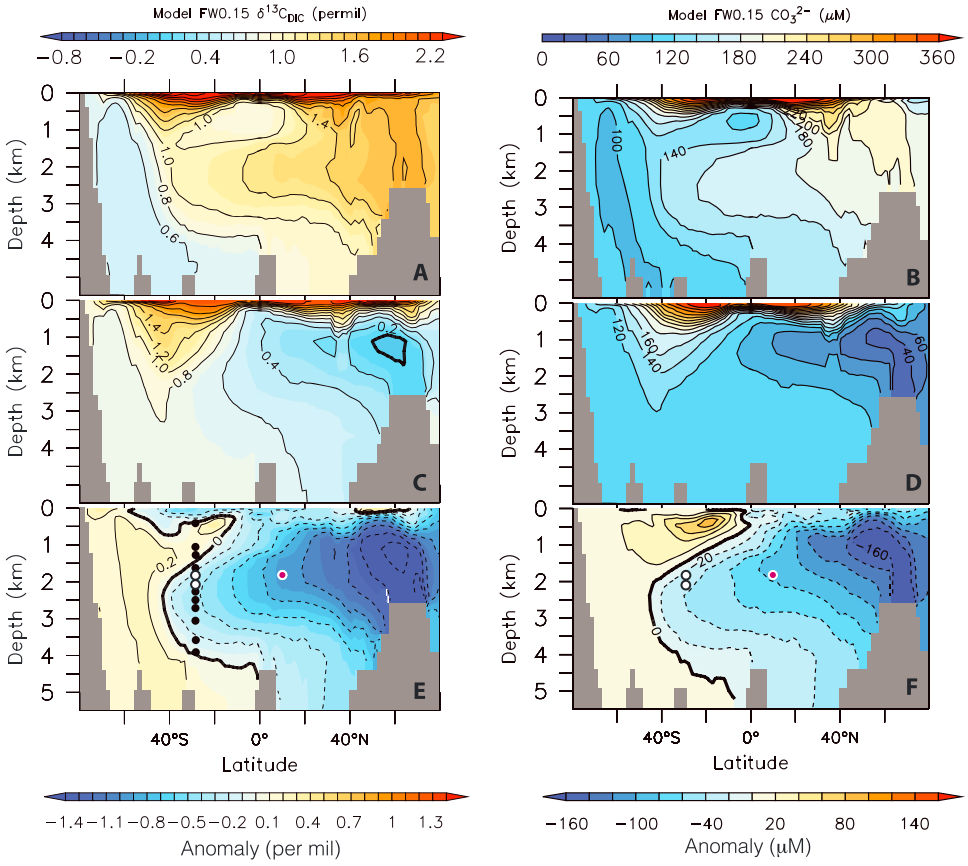

Figure 7. Simulated response of (left-hand column) $\delta^{13}C$ and (right-hand column) [CO_3^{2-}] in the Atlantic due to a freshwater forcing induced AMOC shutdown [*Schmittner and Lund*, 2015]. (a and b) $\delta^{13}C$ and [CO_3^{2-}] for the Atlantic based on preindustrial initial conditions. Note that NADW sits deeper in the water column than would be expected for the LGM given the boundary conditions. (c and d) $\delta^{13}C$ and [CO_3^{2-}] 2500 years after AMOC shutdown. (e and f) The $\delta^{13}C$ and [CO_3^{2-}] anomalies (difference between post-AMOC shutdown and preindustrial values). Both $\delta^{13}C$ and [CO_3^{2-}] show largest decreases in the North Atlantic, with progressively smaller anomalies moving southward. The black circles mark the location of Brazil Margin cores, including the mid-depth sites in white, while the red circle marks the sill depth and latitude associated with VM28-122 [*Yu et al.*, 2010].

At the beginning of the B/A, when the AMOC was apparently reinvigorated, $[CO_3^{2-}]$ increased by 15 μmol/kg at the Brazil Margin, implying that ΣCO_2 declined by ~25 μmol/kg (Figure 3). Vertical $\Delta^{14}C$ gradients in the tropical Atlantic also disappear at the onset of the B/A, consistent with a resumption of the AMOC and enhanced southward advection of ^{14}C enriched NCW [*Chen et al.*, 2015]. Later in the deglaciation, apparent weakening of the AMOC during the YD coincides with a decrease in $[CO_3^{2-}]$ of 10–15 μmol/kg (Figure 3). At the end of the YD, both Pa/Th and coral $\Delta^{14}C$ records imply that the AMOC became reinvigorated once again [*McManus et al.*, 2004; *Chen et al.*, 2015], which should liberate respired carbon from the mid-depth Atlantic. While there was a modest increase in $[CO_3^{2-}]$ at the end of the YD, the signal appears to be lost in the overall glacial-interglacial shift in $[CO_3^{2-}]$, which is likely due to progressively higher preformed DIC values. Lower sedimentation rates and sampling resolution during the YD and early Holocene section of the Brazil Margin cores may also preclude detection of subtle millennial-scale signals during this time interval.

4.3. Spatial Gradients in $[CO_3^{2-}]$ and $\delta^{13}C$ Anomalies During HS1

Model results suggest that weakening of the AMOC should create a north-south gradient in $[CO_3^{2-}]$ anomalies during HS1, similar to that observed in $\delta^{13}C$ [*Schmittner and Lund*, 2015]. Comparison of the Brazil Margin results with $[CO_3^{2-}]$ data from the tropical North Atlantic indicates that there was a meridional gradient in carbonate ion anomalies during HS1, with larger anomalies in the North Atlantic (Figure 6). Although the $[CO_3^{2-}]$ signal in core VM28-122 was originally interpreted as CO_2 released from the deep sea [*Yu et al.*, 2010], we instead suggest that it reflects a weaker AMOC and accumulation of respired carbon at mid-depth, as implied by model results (Figure 7).

While the timing and spatial pattern in $[CO_3^{2-}]$ anomalies are broadly consistent with the expected response to AMOC weakening, inconsistencies between the model results and benthic foraminiferal records do exist. The modeled $[CO_3^{2-}]$ decrease of 20–30 μmol/kg (Figure 7) agrees with the Brazil Margin results, but the model overestimates the observed $[CO_3^{2-}]$ decrease in the tropical North Atlantic by a factor of two. The simulated $\delta^{13}C$ response in the North Atlantic is also larger than implied by observations [*Schmittner and Lund*, 2015]. Either the AMOC did not collapse entirely during HS1 or the use of preindustrial initial conditions amplifies the simulated $[CO_3^{2-}]$ signal at the depth of VM28-122 (~1800 m). In the model simulations, VM28-122 sits in the core of NADW (Figure 7), whereas during the LGM, NCW was shallower in the water column [*Curry and Oppo*, 2005]. As a result, the modeled change in $[CO_3^{2-}]$ during an AMOC shutdown is likely too large for this location. The discrepancy in $[CO_3^{2-}]$ signals may also be due to the lack of interactive carbonate sediment dissolution in the model. Dissolution of $CaCO_3$ under elevated levels of total DIC would increase alkalinity and therefore moderate the $[CO_3^{2-}]$ response. Despite these factors, the observed north-south gradient in $\delta^{13}C$ and $[CO_3^{2-}]$ anomalies is consistent with the accumulation of isotopically light carbon in the mid-depth Atlantic.

4.4. Preformed Versus Remineralized $\delta^{13}C$ Signal

The modeling results of *Schmittner and Lund* [2015] suggest that approximately 65% of the Brazil Margin $\delta^{13}C$ signal can be attributed to remineralized $\delta^{13}C$ ($\delta^{13}C_{Rem}$) and 35% to preformed $\delta^{13}C$ ($\delta^{13}C_{Pre}$) (Figure 8). A somewhat higher proportion of the negative $\delta^{13}C$ shift in the tropical North Atlantic is due to changes in $\delta^{13}C_{Rem}$ (~80%) (Figure 8). Assuming that the $[CO_3^{2-}]$ signal between the LGM (19–21 kyr BP) and early HS1 (16–17 kyr BP) was primarily the result of remineralization, we can estimate the influence on $\delta^{13}C$ using the following mass balance equations:

$$\left(\delta^{13}C_{Final}\right)\left(\Sigma CO_{2\ Final}\right) = \left(\delta^{13}C_{Added}\right)\left(\Sigma CO_{2\ Added}\right) + \left(\delta^{13}C_{LGM}\right)\left(\Sigma CO_{2\ LGM}\right) \quad (1)$$

$$\Sigma CO_{2\ Final} = \Sigma CO_{2\ Added} + \Sigma CO_{2\ LGM} \quad (2)$$

where $\delta^{13}C_{Final}$ represents the $\delta^{13}C$ value after input of respired carbon, $\delta^{13}C_{LGM}$ is the mean $\delta^{13}C$ for the LGM time interval, and $\Sigma CO_{2\ Added}$ is the estimated ΣCO_2 change between the LGM (19–21 kyr BP) and early HS1 (16–17 kyr BP) based on the $[CO_3^{2-}]$ results (Table 2). We assume that $\delta^{13}C_{Added}$ is equal to the mean value for $\delta^{13}C$ for marine organic carbon for samples from 40°S to 80°N (−21 ± 2‰) (2σ) [*Goericke and Fry*, 1994]. Although we have no proxy estimate for $\Sigma CO_{2\ LGM}$, the mean ΣCO_2 for the modern global ocean below 1000 m water depth is 2270 ± 50 μmol/kg (1σ) [*Schmittner et al.*, 2013]. We assume a similar value for the LGM but with a

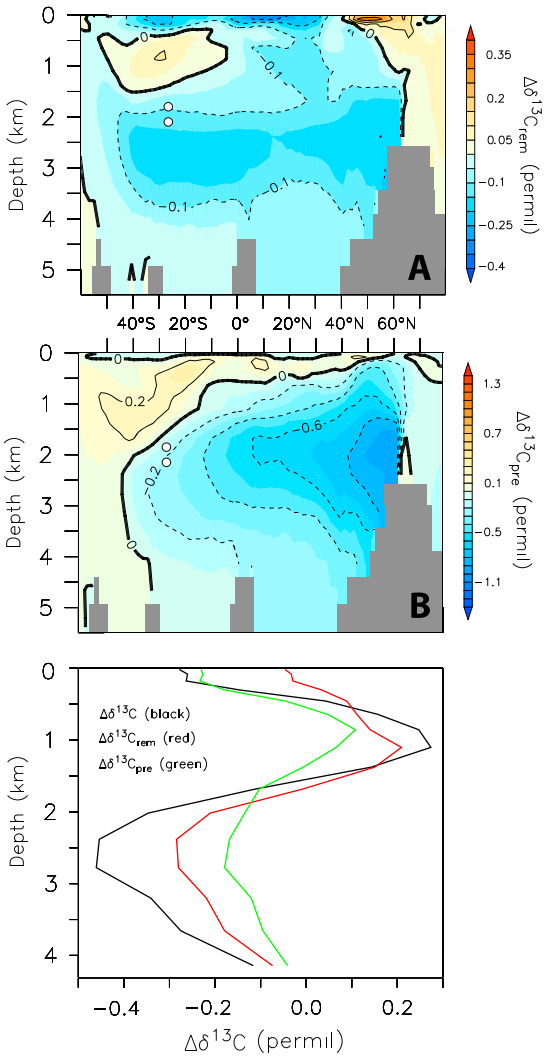

Figure 8. Simulated changes in $\Delta\delta^{13}C_{pre}$ and $\Delta\delta^{13}C_{rem}$ due to a freshwater forcing induced shutdown of the AMOC [*Schmittner and Lund*, 2015]. (a) Zonally averaged $\Delta\delta^{13}C_{pre}$ for the Atlantic basin. The approximate location of the mid-depth Brazil Margin cores is noted with white circles. (b) Zonally averaged $\Delta\delta^{13}C_{rem}$ for the Atlantic basin. (c) Average $\Delta\delta^{13}C$ (black), $\Delta\delta^{13}C_{pre}$ (green), and $\Delta\delta^{13}C_{rem}$ (red) at 28°S, using vertical profiles from 30°W to 45°W. The remineralized signal is approximately double the preformed signal at the depth of the Brazil Margin cores. Note that the anomalies are calculated 1000 years after the AMOC collapse to facilitate comparison to the HS1 $\delta^{13}C$ anomalies, which were determined using the 16–17 kyr BP time window.

conservative ±100 μmol/kg uncertainty. Note that the exact choice for $\Sigma CO_{2\ LGM}$ has little influence on $\delta^{13}C_{Final}$ because of the modest relative error of ~5%.

The mass balance results imply that most of the Brazil Margin $\delta^{13}C$ signal was due to changes in $\delta^{13}C_{Rem}$. For example, $\delta^{13}C_{Final}$ for 78GGC is 0.68‰, which means that ~75% of the change between the LGM ($\delta^{13}C$ = 1.03‰) and early HS1 ($\delta^{13}C$ = 0.55‰) can be attributed to remineralization. Taking into account the errors listed in Table 1, the proportion due to remineralization ranges from 50% to 100%. A somewhat lower fraction of the HS1 $\delta^{13}C$ signal in core 33GGC can be explained by changes in $\delta^{13}C_{Rem}$ (65%), but it is within error of the 78GGC results. In the North Atlantic, it appears that remineralization also caused ~75% of the HS1 $\delta^{13}C$ signal, with the proportion ranging from 50% to 100%. Thus, the results from each core show that remineralization played the primary role in setting the $\delta^{13}C$ tracer field at mid-depths, consistent with our model results (Figure 8).

The remainder of the $\delta^{13}C$ signal at each site must be due to changes in $\delta^{13}C_{Pre}$. We estimate that the $\delta^{13}C_{Pre}$ signal was −0.13 ± 0.11‰ for 78GGC, −0.13 ± 0.16‰ for 33GGC, and −0.14 ± 0.16‰ for VM28-122. These values are similar to the modeled ~0.15‰ decrease in $\delta^{13}C_{Pre}$ in the mid-depth Atlantic (Figure 8), which is driven by gas

Table 2. Mass Balance Parameters and Results

	KNR159-5-78GGC[a]	KNR159-5-33GGC[a]	VM28-122[b]
Mean LGM $\delta^{13}C$ (‰)	1.03 ± 0.01	0.77 ± 0.02	1.1 ± 0.04
$\Sigma CO_{2\ Added}$ (μmol/kg)	37 ± 4	23 ± 6	48 ± 7
$\delta^{13}C_{Final}$ (‰)	0.68 ± 0.10	0.55 ± 0.16	0.64 ± 0.12
Mean HS1 $\delta^{13}C$ (‰)	0.55 ± 0.02	0.43 ± 0.02	0.5 ± 0.1

[a] $\delta^{13}C$ from *Tessin and Lund* [2013].
[b] $\delta^{13}C$ from *Oppo and Fairbanks* [1987] and *Yu et al.* [2010].

exchange with a ^{13}C-depleted atmosphere and weakening of the biological pump triggered by shutdown of the AMOC, both of which cause surface ocean $\delta^{13}C$ to decrease [*Schmittner and Lund*, 2015]. The overall agreement between the reconstructed and modeled values for $\delta^{13}C_{Rem}$ and $\delta^{13}C_{Pre}$ suggests (1) weakening of the AMOC drove changes in both remineralized and preformed $\delta^{13}C$ to yield the overall HS1 $\delta^{13}C$ anomalies and (2) the majority of the $\delta^{13}C$ response was due to biological processes, implying that $\delta^{13}C$ acted nonconservatively during HS1. Our results are consistent with previous indications of nonconservative $\delta^{13}C$ behavior during the last deglaciation [e.g., *Tessin and Lund*, 2013; *Oppo et al.*, 2015] and to our knowledge provide the first quantitative estimate of preformed and remineralized $\delta^{13}C$ components using paired stable isotope and B/Ca results.

4.5. Implications for Atmospheric CO_2

If a weakened AMOC resulted in greater carbon storage in the mid-depth Atlantic during HS1 and YD, what is the fate of the sequestered carbon under a reinvigorated AMOC circulation, and what are the implications for atmospheric CO_2? Two centennial scale ~10–15 ppm increases in atmospheric CO_2 occurred at ~14.8 and ~11.7 kyr BP [*Marcott et al.*, 2014] (Figure 3). *Bauska et al.* [2016] report minor shifts in the $\delta^{13}C$ of atmospheric-CO_2 associated with the centennial-scale events. Given that the abrupt increases in CO_2 coincide with northern hemisphere warming, SST may be the primary driver, with contributions from other secondary inputs that moderate the $\delta^{13}C$ signal [*Bauska et al.*, 2016]. The relative timing of the centennial scale events with abrupt reinvigoration of the AMOC implies that there is tight coupling between the overturning circulation and pCO_2 variability [*Marcott et al.*, 2014]. The resumption of the AMOC may trigger abrupt liberation of CO_2 to the atmosphere as a result of changes in terrestrial carbon storage [*Köhler et al.*, 2005]. Alternatively, *Chen et al.* [2015] hypothesized that the abrupt increases in CO_2 were due to flushing of remineralized carbon out of the mid-depth Atlantic during intervals of reinvigorated overturning. Consistent with this idea, our data suggest that ΣCO_2 decreased at the end of HS1 (Figure 3). Our data also show that carbon accumulated at mid-depths during the course of HS1, which would tend to draw down atmospheric CO_2. Thus, it is unlikely that the mid-depth Atlantic acted as a net source of carbon to the atmosphere across the combined HS1 to B-A interval. Instead, we suggest that sequestration in the mid-depth Atlantic muted the rate of atmospheric CO_2 rise during HS1. Upon the resumption of overturning during the B-A, we speculate that the accumulated carbon was then released, rectifying the deficit in atmospheric CO_2 caused by the weakened AMOC state. A similar process may have occurred during the YD, where weakening of the AMOC resulted in carbon sequestration and lower [CO_3^{2-}] at mid-depths (Figure 3). Presumably, reinvigoration of the AMOC at the end of the YD caused the carbon to be released, which may contribute to the observed abrupt shift in atmospheric CO_2 at 11.7 kyr BP [*Marcott et al.*, 2014; *Chen et al.*, 2015].

Our results imply that other factors, such as weakening of the biological pump [*Schmittner and Lund*, 2015; *Hertzberg et al.*, 2016] or release of CO_2 from the Southern Ocean [*Anderson et al.*, 2009], must have caused the rise in atmospheric CO_2 during HS1 and the YD, overcoming the temporary carbon sink in the mid-depth Atlantic. The combined effects of a weakened biological pump and release of respired carbon may explain why atmospheric CO_2 increased in a stepwise pattern, instead of a steady monotonic fashion throughout the deglaciation. AMOC-related changes in the carbon cycle cannot explain the overall increase in pCO_2; additional processes must be involved in maintaining high CO_2 levels during the B-A and Holocene when the AMOC was robust and the global preformed nutrient budget would presumably favor carbon sequestration in the ocean interior [*Galbraith and Jaccard*, 2015].

4.6. Quantifying ΣCO_2 Storage

To assess whether the release of respired carbon could have contributed to the centennial-scale increase in atmospheric CO_2 at the end of HS1, we use the B/Ca records from the Brazil Margin and tropical North Atlantic to generate an initial quantitative estimate of ΣCO_2 storage. We assume that ALK remained constant from the LGM to HS1. As noted above, this will likely yield a minimum estimate for ΣCO_2 given that (1) carbonate dissolution would increase alkalinity and minimize the [CO_3^{2-}] signal and (2) enhanced residence time of mid-depth water during HS1 would lead to accumulation of alkalinity associated with the hard tissue pump (Figure 5). We assume a depth range of 1750 ± 250 m and an area of 5.2 ± 0.3 × 10^{13} m^2 (~60°N to ~35°S), which is the approximate volume encompassed by negative $\delta^{13}C$ anomalies in a simulated

shutdown of the AMOC [*Schmittner and Lund*, 2015]. Using a seawater density of 1026 kg/m^3, this volume is equivalent to a total mass of 9.3 ± 1.4 × 10^{19} kg. Assuming an average decrease in [CO_3^{2-}] from the LGM to HS1 of 30 ± 10 μmol/kg, we estimate an average increase in ΣCO_2 of 50 ± 17 μmol/kg or a total carbon storage of 56 ± 21 Pg.

If 56 Pg of carbon was released directly to the atmosphere, it would be equivalent to a pCO_2 change of ~26 ppm (1 ppm–2.12 Gt C [*Keeling and Whorf*, 2005]). A portion of this carbon would be reabsorbed by the upper ocean, however, so the net influence on atmospheric CO_2 would be substantially less. Over the past two centuries, 50% of the carbon released through fossil fuel burning has been absorbed by the ocean [*Sabine et al.*, 2004]. To first order, we would expect a similar proportion to be absorbed by the ocean during centennial-scale CO_2 events of the last deglaciation. Determining the actual fate of the stored carbon will require detailed modeling efforts to assess the proportions released to the atmosphere and redistributed to other ocean basins. Additional remineralized organic carbon may have been stored in the deep Atlantic (>2500 m) prior to HS1 [*Hoogakker et al.*, 2015; *Howe et al.*, 2016], which should also be considered in assessing redistribution of carbon between various reservoirs. Given the uncertainties in our estimate of ΣCO_2 storage, additional high-resolution B/Ca records from a range of depths and locations will be necessary to refine estimates for the Atlantic. Nevertheless, our initial estimate suggests that significant quantities of carbon were stored in the mid-depth Atlantic during HS1 and the YD and the mid-depth reservoir should be taken into account when interpreting the atmospheric CO_2 signal during the last deglaciation.

4.7. Glacial-Interglacial Changes in [CO_3^{2-}]

The dominant long-term trend in the Brazil Margin records is a steady decrease in [CO_3^{2-}] from the LGM to the early Holocene (Figure 2). The most likely explanation for the signal is changing preformed ΣCO_2 due to air-sea exchange with an atmosphere with progressively higher CO_2 levels. Although air-sea gas exchange is an unlikely driver for the millennial-scale decreases in [CO_3^{2-}] during HS1 and the YD, over the course of the deglaciation, such a process could lead to lower [CO_3^{2-}] at depths influenced by NCW. For example, after the rapid decline in [CO_3^{2-}] during HS1, [CO_3^{2-}] rebounds during the B-A but does not fully recover to LGM values (Figure 3). This suggests that preformed ΣCO_2 in the mid-depth Atlantic increased as a result of greater CO_2 absorption from the atmosphere. Between the LGM and B-A, atmospheric CO_2 increased by ~50 ppm. A decline in global ocean alkalinity may also contribute to the long-term [CO_3^{2-}] trend at the Brazil Margin. Although there was little apparent change in carbonate weathering [*Foster and Vance*, 2006] and deep-sea $CaCO_3$ burial [*Catubig et al.*, 1998] on glacial-interglacial time scales, flooding of continental shelves late in the deglaciation would facilitate deposition in carbonate banks and coral reefs, removing ALK and DIC in a 2:1 ratio [*Sigman and Boyle*, 2000]. Thus, a portion of the deglacial [CO_3^{2-}] decline in the Brazil Margin records may reflect ALK removal.

If the long-term [CO_3^{2-}] trend at the Brazil Margin responded primarily to atmospheric CO_2 and global changes in alkalinity, then we would expect little change in [CO_3^{2-}] once atmospheric CO_2 and sea level stabilized in the early Holocene. While this is largely the case at 2100 m water depth, [CO_3^{2-}] at 1800 m steadily increased from 10 to 2 kyr BP (Figure 2). One possible explanation of the depth-dependent signal is a shift in water mass geometry. During the LGM, [CO_3^{2-}] was ~10 μmol/kg higher at 1800 m than at 2100 m (Figure 3), which is consistent with Brazil Margin $\delta^{13}C$ profiles that show that the core of NCW was located at 1600–1800 m water depth [*Lund et al.*, 2015]. By the early Holocene, however, [CO_3^{2-}] was 10–15 μmol/kg *lower* at 1800 m than 2100 m and vertical $\delta^{13}C$ profiles suggest that the core of NCW had migrated to 2000–2500 m [*Lund et al.*, 2015]. Thus, the 1800 m core site would have been more heavily influenced by high [CO_3^{2-}] NCW during the LGM than during the early Holocene, potentially accounting for the different temporal trend at this water depth. Additional factors, such as enhanced Labrador Sea Water formation [*Hoogakker et al.*, 2011] and the appearance of Upper Circumpolar Deep Water at the Brazil Margin during the mid-Holocene [*Lund et al.*, 2015], likely influence the long-term evolution of the mid-depth [CO_3^{2-}] signal. Detailed vertical transects of B/Ca from the Brazil Margin and elsewhere are necessary to more fully assess the roles of rising atmospheric CO_2, global alkalinity, and vertical migration of water mass boundaries on the glacial-interglacial [CO_3^{2-}] signal.

5. Conclusions

Carbon isotope anomalies were a ubiquitous feature of the mid-depth Atlantic during HS1, yet the driver of the anomalies has remained enigmatic. Recent modeling efforts suggest that the $\delta^{13}C$ signal is driven by weakening of the AMOC that increases the residence time of mid-depth waters, allowing for the accumulation of isotopically light respired carbon. Here we examined the ΣCO_2 history at ~2 km water depth in the South Atlantic using two high-resolution B/Ca time series spanning the last ~25 kyr. Our records show that $[CO_3^{2-}]$ decreased by 20–25 μmol/kg during HS1, concomitant with apparent weakening of the AMOC. The records also show that $[CO_3^{2-}]$ increased ~15 μmol/kg during the B-A and decreased ~15 μmol/kg during the YD, suggesting a tight coupling between mid-depth $[CO_3^{2-}]$ and AMOC state. Given the inverse relationship between $[CO_3^{2-}]$ and ΣCO_2, we infer that ΣCO_2 increased during millennial-scale stadial events of the last deglaciation. We also present model results that indicate weakening of the AMOC increases alkalinity at mid-depths, implying the $[CO_3^{2-}]$ time series likely underestimate the ΣCO_2 signal.

Comparison of the $[CO_3^{2-}]$ results from the Brazil Margin and tropical North Atlantic indicates that there was a meridional gradient in $[CO_3^{2-}]$ anomalies during HS1, similar to the pattern observed in $\delta^{13}C$ records. Our mass balance estimates suggest that approximately 75% of the $\delta^{13}C$ signal at 27°S and 12°N was due to remineralization, highlighting the nonconservative nature of $\delta^{13}C$ behavior during HS1. Given that simulated weakening of the AMOC produces analogous spatial patterns in $[CO_3^{2-}]$ and $\delta^{13}C$, we infer that the dominant driving mechanism behind the observed signals is the accumulation of remineralized carbon.

Our results imply the mid-depth Atlantic sequestered carbon during HS1 and the YD, both times of rising atmospheric CO_2. Thus, alternative processes, such as weakening of the biological pump [*Hertzberg et al.*, 2016] or outgassing from the Southern Ocean [*Anderson et al.*, 2009], must account for the overall increase in atmospheric CO_2 during stadial events. Reinvigoration of the AMOC may release stored carbon from the mid-depth Atlantic and contribute to abrupt centennial-scale increases in CO_2 at the end of HS1 and the YD. The decrease in ΣCO_2 at the Brazil Margin at the beginning of the B-A is consistent with this scenario. We also present a preliminary estimate of carbon storage in the mid-depth Atlantic comparable to the quantity required to account for the rise in atmospheric CO_2 at the end of HS1. Determining the fate of the stored carbon will require detailed modeling efforts to assess partitioning between atmospheric and oceanic reservoirs.

Acknowledgments

We would like to thank Graham Nash at Australian National University for his help with sample processing and Jennifer Hertzberg for reviewing a presubmission version of this manuscript. Two anonymous reviewers also made substantive comments that greatly improved the final version. We are grateful to the WHOI core lab for sample collection and archiving. This work was supported by NSF grant OCE-1404915 to D.L. and by ARC Discovery Project DP140101393 and Future Fellowship FT140100993 to J.Y. The data presented in this paper are available at https://www.ncdc.noaa.gov/paleo/study/22090.

References

Anderson, R. F., S. Ali, L. I. Bradtmiller, S. H. Nielsen, M. Q. Fleisher, B. E. Anderson, and L. H. Burckle (2009), Wind-driven upwelling in the Southern Ocean and the deglacial rise in atmospheric CO_2, *Science*, *323*(5920), 1443–1448.

Angulo, R. J., M. C. de Souza, P. J. Reimer, and S. K. Sasaoka (2005), Reservoir effect of the southern and southeastern Brazilian coast, *Radiocarbon*, *47*(1), 67–73.

Annan, J., and J. Hargreaves (2013), A new global reconstruction of temperature changes at the Last Glacial Maximum, *Clim. Past*, *9*(1), 367–376.

Bauska, T. K., D. Baggenstos, E. J. Brook, A. C. Mix, S. A. Marcott, V. V. Petrenko, H. Schaefer, J. P. Severinghaus, and J. E. Lee (2016), Carbon isotopes characterize rapid changes in atmospheric carbon dioxide during the last deglaciation, *Proc. Natl. Acad. Sci. U.S.A.*, *113*(13), 3465–3470.

Catubig, N. R., D. E. Archer, R. Francois, P. deMenocal, W. Howard, and E.-F. Yu (1998), Global deep-sea burial rate of calcium carbonate during the Last Glacial Maximum, *Paleoceanography*, *13*, 298–310, doi:10.1029/98PA00609.

Chen, T., L. F. Robinson, A. Burke, J. Southon, P. Spooner, P. J. Morris, and H. C. Ng (2015), Synchronous centennial abrupt events in the ocean and atmosphere during the last deglaciation, *Science*, *349*(6255), 1537–1541.

Clark, P. U., A. S. Dyke, J. D. Shakun, A. E. Carlson, J. Clark, B. Wohlfarth, J. X. Mitrovica, S. W. Hostetler, and A. M. McCabe (2009), The Last Glacial Maximum, *Science*, *325*(5941), 710–714.

Curry, W. B., and D. W. Oppo (2005), Glacial water mass geometry and the distribution of $\delta^{13}C$ of ΣCO_2 in the western Atlantic Ocean, *Paleoceanography*, *20*, PA1017, doi:10.1029/2004PA001021.

Curry, W. B., J. Duplessy, L. Labeyrie, and N. J. Shackleton (1988), Changes in the distribution of $\delta^{13}C$ of deep water ΣCO_2 between the last glaciation and the Holocene, *Paleoceanography*, *3*, 317–341, doi:10.1029/PA003i003p00317.

Dokken, T. M., and E. Jansen (1999), Rapid changes in the mechanism of ocean convection during the last glacial period, *Nature*, *401*(6752), 458–461.

Duplessy, J., N. Shackleton, R. Fairbanks, L. Labeyrie, D. Oppo, and N. Kallel (1988), Deepwater source variations during the last climatic cycle and their impact on the global deepwater circulation, *Paleoceanography*, *3*, 343–360, doi:10.1029/PA003i003p00343.

Foster, G. L., and D. Vance (2006), Negligible glacial-interglacial variation in continental chemical weathering rates, *Nature*, *444*, 918–921.

Galbraith, E. D., and S. L. Jaccard (2015), Deglacial weakening of the oceanic soft tissue pump: Global constraints from sedimentary nitrogen isotopes and oxygenation proxies, *Quat. Sci. Rev.*, *109*, 38–48.

Gherardi, J., L. Labeyrie, S. Nave, R. Francois, J. F. McManus, and E. Cortijo (2009), Glacial-interglacial circulation changes inferred from $^{231}Pa/^{230}Th$ sedimentary record in the North Atlantic region, *Paleoceanography*, *24*, PA2204, doi:10.1029/2008PA001696.

Goericke, R., and B. Fry (1994), Variations of marine plankton $\delta^{13}C$ with latitude, temperature, and dissolved CO_2 in the world ocean, *Global Biogeochem. Cycles*, *8*, 85–90, doi:10.1029/93GB03272.

Hayes, C. T., et al. (2015), ^{230}Th and ^{231}Pa on GEOTRACES GA03, the US GEOTRACES North Atlantic transect, and implications for modern and paleoceanographic chemical fluxes, *Deep Sea Res., Part II*, *116*, 29–41.

Hertzberg, J. E., D. C. Lund, A. Schmittner, and A. Srkrivanek (2016), Evidence for a biological pump driver of atmospheric CO_2 rise during Heinrich Stadial 1, *Geophys. Res. Lett.*, *43*, 12,242–12,251, doi:10.1002/2016GL070723.

Hoffman, J., and D. Lund (2012), Refining the stable isotope budget for Antarctic bottom water: New foraminiferal data from the abyssal Southwest Atlantic, *Paleoceanography*, *27*, PA1213, doi:10.1029/2011PA002216.

Hoogakker, B. A. A., M. R. Chapman, I. N. McCave, C. Hillaire-Marcel, C. R. W. Ellison, I. R. Hall, and R. J. Telford (2011), Dynamics of North Atlantic deep water masses during the Holocene, *Paleoceanography*, *26*, PA4214, doi:10.1029/2011PA002155.

Hoogakker, B. A. A., et al. (2015), Glacial-interglacial changes in bottom-water oxygen content on the Portuguese margin, *Nat. Geosci.*, *8*(1), 40–43.

Howe, J. N. W., A. M. Piotrowski, T. L. Noble, S. Mulitza, C. M. Chiessi, and G. Bayon (2016), North Atlantic deep water production during the Last Glacial Maximum, *Nat. Commun.*, doi:10.1038/ncomms11765.

Huang, K.-F., D. W. Oppo, and W. B. Curry (2014), Decreased influence of Antarctic intermediate water in the tropical Atlantic during North Atlantic cold events, *Earth Planet. Sci. Lett.*, *389*, 200–208.

Köhler, P., F. Joos, S. Gerber, and R. Knutti (2005), Simulated changes in vegetation distribution, land carbon storage, and atmospheric CO_2 in response to a collapse of the North Atlantic thermohaline circulation, *Clim. Dyn.*, *25*, 689–708.

Kroopnick, P. (1985), The distribution of $\delta^{13}C$ of ΣCO^2 in the world oceans, *Deep Sea Res., Part A*, *32*(1), 57–84.

Keeling, C. D., and T. P. Whorf (2005), Atmospheric carbon dioxide record from Mauna Loa, in *Carbon Dioxide Research Group, Scripps Institution of Oceanography*, Univ. of Calif. La Jolla, doi:10.3334/CDIAC/atg.035.

Lewis, E., D. Wallace, and L. J. Allison (2014), Program developed for CO_2 system calculations carbon dioxide information analysis center, Managed by Lockheed Martin Energy Research Corporation for the US Department of Energy Tennessee.

Lourantou, A., J. V. Lavrič, P. Köhler, J.-M. Barnola, D. Paillard, E. Michel, D. Raynaud, and J. Chappellaz (2010), Constraint on the CO_2 rise by new atmospheric carbon isotopic measurements during the last deglaciation, *Global Biogeochem. Cycles*, *24*, GB2015, doi:10.1029/2009GB003545.

Lund, D., A. Tessin, J. Hoffman, and A. Schmittner (2015), Southwest Atlantic water mass evolution during the last deglaciation, *Paleoceanography*, *30*, 477–494, doi:10.1002/2014PA002657.

Lynch-Stieglitz, J., T. F. Stocker, W. S. Broecker, and R. G. Fairbanks (1995), The influence of air-sea exchange on the isotopic composition of oceanic carbon: Observations and modeling, *Global Biogeochem. Cycles*, *9*, 653–665, doi:10.1029/95GB02574.

Marcott, S. A., et al. (2014), Centennial-scale changes in the global carbon cycle during the last deglaciation, *Nature*, *514*(7524), 616–619.

McManus, J. F., D. W. Oppo, and J. L. Cullen (1999), A 0.5-million-year record of millennial-scale climate variability in the North Atlantic, *Science*, *283*(5404), 971–975.

McManus, J. F., R. Francois, J. Gherardi, L. D. Keigwin, and S. Brown-Leger (2004), Collapse and rapid resumption of Atlantic meridional circulation linked to deglacial climate changes, *Nature*, *428*(6985), 834–837.

Oppo, D. W., and R. G. Fairbanks (1987), Variability in the deep and intermediate water circulation of the Atlantic Ocean during the past 25,000 years: Northern Hemisphere modulation of the Southern Ocean, *Earth Planet. Sci. Lett.*, *86*(1), 1–15.

Oppo, D. W., W. B. Curry, and J. F. McManus (2015), What do benthic $\delta^{13}C$ and $\delta^{18}O$ data tell us about Atlantic circulation during Heinrich Stadial 1?, *Paleoceanography*, *30*, 353–368, doi:10.1002/2014PA002667.

Praetorius, S. K., et al. (2008), Episodic reductions in bottom-water currents since the last ice age, *Nat. Geosci.*, *1*(7), 449–452.

Rickaby, R., and H. Elderfield (2005), Evidence from the high-latitude North Atlantic for variations in Antarctic intermediate water flow during the last deglaciation, *Geochem. Geophys. Geosyst.*, *6*, Q05001, doi:10.1029/2004GC000858.

Sabine, C. L., et al. (2004), The oceanic sink for anthropogenic CO_2, *Science*, *305*, 367–371.

Schlitzer, R. (2015), Ocean Data View. [Available at http://odv.awi.de.]

Schmitt, J., et al. (2012), Carbon isotope constraints on the deglacial CO_2 rise from ice cores, *Science*, *336*(6082), 711–714.

Schmittner, A., and D. Lund (2015), Early deglacial Atlantic overturning decline and its role in atmospheric CO_2 rise inferred from carbon isotopes ($\delta^{13}C$), *Clim. Past*, *11*(2), 135–152.

Schmittner, A., N. Gruber, A. Mix, R. Key, A. Tagliabue, and T. Westberry (2013), Biology and air-sea gas exchange controls on the distribution of carbon isotope ratios ($\delta^{13}C$) in the ocean, *Biogeosciences*, *10*(9), 5793–5816.

Schneider, B., G. Leduc, and W. Park (2010), Disentangling seasonal signals in Holocene climate trends by satellite-model-proxy integration, *Paleoceanography*, *25*, PA4217, doi:10.1029/2009PA001893.

Schneider, R., A. Dahmke, A. Kölling, P. Müller, H. Schulz, and G. Wefer (1992), Strong deglacial minimum in the δ13C record from planktonic foraminifera in the Benguela upwelling region: Palaeoceanographic signal or early diagenetic imprint?, *Geol. Soc. London, Spec. Publ.*, *64*(1), 285–297.

Shakun, J. D., P. U. Clark, F. He, S. A. Marcott, A. C. Mix, Z. Liu, B. Otto-Bliesner, A. Schmittner, and E. Bard (2012), Global warming preceded by increasing carbon dioxide concentrations during the last deglaciation, *Nature*, *484*(7392), 49–54.

Sigl, M., et al. (2016), The WAIS-divide deep ice core WD2014 chronology—Part 1: Annual layer counting (31–0 ka B.P.), *Clim. Past Discuss.*, *12*, 769–786.

Sigman, D. M., and E. A. Boyle (2000), Glacial/interglacial variations in atmospheric carbon dioxide, *Nature*, *407*(6806), 859–869.

Tessin, A., and D. Lund (2013), Isotopically depleted carbon in the mid-depth South Atlantic during the last deglaciation, *Paleoceanography*, *28*, 296–306, doi:10.1002/palo.20026.

Thornalley, D. J., H. Elderfield, and I. N. McCave (2010), Intermediate and deep water paleoceanography of the northern North Atlantic over the past 21,000 years, *Paleoceanography*, *25*, PA1211, doi:10.1029/2009PA001833.

Waelbroeck, C., L. Skinner, L. Labeyrie, J. Duplessy, E. Michel, N. Vazquez Riveiros, J.-M. Gherardi, and F. Dewilde (2011), The timing of deglacial circulation changes in the Atlantic, *Paleoceanography*, *26*, PA3213, doi:10.1029/2010PA002007.

Weaver, A. J., M. Eby, A. F. Fanning, and E. C. Wiebe (1998), Simulated influence of carbon dioxide, orbital forcing and ice sheets on the climate of the Last Glacial Maximum, *Nature*, *394*(6696), 847–853.

Xie, R. C., F. Marcantonio, and M. W. Schmidt (2012), Deglacial Variability of Antarctic Intermediate Water Penetration into the North Atlantic from Authigenic Neodymium Isotope Ratios, *Paleoceanography*, *27*, PA3221, doi:10.1029/2012PA002337.

Yu, J., and H. Elderfield (2005), B/Ca in foraminiferal calcium carbonate and its potential as a paleo-pH proxy, Abstract PP11B-1451 presented at 2005 Fall Meeting, AGU, San Francisco, Calif.

Yu, J., and H. Elderfield (2007), Benthic foraminiferal B/Ca ratios reflect deep water carbonate saturation state, *Earth Planet. Sci. Lett.*, *258*(1), 73–86.

Yu, J., H. Elderfield, and A. M. Piotrowski (2008), Seawater carbonate ion-$\delta^{13}C$ systematics and application to glacial–interglacial North Atlantic ocean circulation, *Earth Planet. Sci. Lett.*, *271*(1), 209–220.

Yu, J., W. S. Broecker, H. Elderfield, Z. Jin, J. McManus, and F. Zhang (2010), Loss of carbon from the deep sea since the Last Glacial Maximum, *Science*, *330*(6007), 1084–1087.

Yu, J., et al. (2016), Sequestration of carbon in the deep Atlantic during the last glaciation, *Nat. Geosci.*, *9*, 319–324, doi:10.1038/NGEO2657.

Zahn, R., and A. Stüber (2002), Suborbital intermediate water variability inferred from paired benthic foraminiferal Cd/Ca and $\delta^{13}C$ in the tropical West Atlantic and linking with North Atlantic climates, *Earth Planet. Sci. Lett.*, *200*(1), 191–205.

Zahn, R., J. Schönfeld, H. Kudrass, M. Park, H. Erlenkeuser, and P. Grootes (1997), Thermohaline instability in the North Atlantic during meltwater events: Stable isotope and ice-rafted detritus records from core SO75-26KL, Portuguese margin, *Paleoceanography*, *12*, 696–710, doi:10.1029/97PA00581.